# Far-travelled ash in past and future eruptions: Combining tephrochronology with volcanic studies

*Running title: Volcanology and tephrochronology*

Katharine V. Cashman and Alison C. Rust
University of Bristol, School of Earth Sciences, Bristol BS8 1RJ, UK

## Abstract

Studies of recent eruptions have improved our understanding of volcanic ash transport and deposition, but have also raised important questions about the behavior of far-travelled (distal) volanic ash. In particular, it is difficult to reconcile estimates of distal ash mass and transport distance determined from eyewitness accounts, mapped deposits, satellite-based observations, and cryptotephra records. Here we address this problem using data from well-characterized eruptions that, collectively, include all four data types. Data from recent eruptions allow us to relate eyewitness accounts to mapped deposits on the ground and satellite-based observations of ash in the air; observations from an historic eruption link eyewitness accounts to cryptotephra deposits. Together these examples show that (1) 10-20% of the erupted mass is typically deposited outside the mapped limits; (2) estimates of the ash mass transported in volcanic clouds cannot account for all of this unmapped ash; and (3) ash fall observed at distances beyond mapped deposits can have measurable impacts, and can form cryptotephra deposits with high ($>\sim 1000/cm^3$) shard counts. We conclude that cryptotephra data can be incorporated into volcanological studies of ash transport and deposition and provide important insight into both the behavior and impacts of far-travelled volcanic ash particles.

*Keywords:* volcanic ash, cryptotephra, ash dispersion models, tephrochronology

## Introduction

The impacts of far-travelled (>1000 km) volcanic ash on northern Europe were highlighted in 2010 and 2011 with the eruptions of Eyjafjallajökull and Grimsvötn volcanoes, Iceland, and related disruption to aviation. These eruptions underlined past cautions about the frequent transport of Icelandic ash to Europe (Thorarinsson, 1981) and have prompted assessments of future ash hazards from eruptions in Iceland (Swindles et al., 2011; Lawson et al., 2012; Watson et al., 2017) and North America (Jensen et al., 2014; Bourne et al., 2016; Plunkett and Pilcher, 2018). Observations from these eruptions also highlight differences in the ways that the volcanological, remote sensing and tephrochronology communities collect and analyze volcanic ash data. Here we explore these differences with the goal of determining the extent to which cryptotephra data, in particular, can be used to improve volcanological studies of far-travelled volcanic ash. At the same time, we test an underlying assumption of cryptotephra analysis, which is that small accumulations of ash shards at distances >1000 km from source vents represent primary deposits of individual eruptions. We compare some combination of eyewitness accounts, deposit data, satellite-based observations and the cryptotephra record from three well-observed recent eruptions (Mount St. Helens, 1980; Pinatubo, 1991; Eyjafjallajökull, 2010), one well observed past eruption (Askja 1875), and one large eruption with widely dispersed cryptotephra (860 CE White River Ash). We use these examples to demonstrate the impacts of far-travelled ash and to illustrate the types of hazard information that can be obtained from cryptotephra data, including ways to improve models of ash transport and deposition (e.g., Saxby et al., this volume).

## Background

A primary tool of physical volcanology is mapping and characterizing tephra deposits on the ground to determine the magnitude (volume) and intensity (eruption rate) of the associated volcanic activity (Pyle, 1989). Deposit maps also provide the basis for probabilistic models of future ash hazards (e.g, Cioni et al., 2003; Jenkins et al., 2015). The most common measurement of visible deposits is thickness. With sufficient spatial coverage, thickness data can be contoured to create isopach maps that, in turn, can be used to estimate the total deposit volume. Deposits from recent well-observed eruptions have been mapped to >500 km from the vent and to a thickness of 0.5 cm or less (Sarna-Wojcicki et al., 1981; McGimsey et al., 1996; Wiesner et al., 2004; Watt et al., 2009). Far-travelled ash is not routinely included in isopach maps of past eruptions, however, because distal ash deposits are too thin to be preserved as coherent layers, although the mass proportion of this far-travelled ash can be significant. For example, Fierstein and Nathenson (1992) calculate this "missing" ash volume by extrapolating mapped isopachs and assuming exponential thinning (Thorarinsson, 1967; Pyle, 1989). This approach suggests that the unmapped deposit may comprise 10-20%, and in some cases >30%, of the total erupted mass. Alternative models for thickness distributions (power law, Weibull; Bonadonna and Costa, 2012) yield even higher missing ash proportions. Improving our understanding of this far-travelled ash is important (1) to test models for deposit thinning, and hence improve estimates of eruption parameters, (2) to constrain the mass fraction of volcanic ash employed in model forecasts of volcanic clouds (e.g.,

Beckett et al., 2015), and (3) to assess potential distal ash impacts of future eruptions, particularly very large events.

Complementary views of far-travelled ash are provided by eyewtiness accounts and satellite observations of volcanic clouds. Systematic compilations of syn-eruptive ash fall observations are surprisingly rare, particularly in distal environments, but exist for a few older (e.g., 1875 Askja, Iceland; Thorarinsson, 1981; 1902 Santa Maria, Guatemala; Sapper, 1904; 1932 Quizapu; Larsson, 1937) and recent (1980, Mount St. Helens; Eychenne et al., 2015) eruptions. Satellite-based measurements of ash clouds, in contrast, are now routine and permit volcanic clouds to be tracked over 1000s of km, and for days after the end of an eruption (e.g., Mackie et al., 2016; Prata and Lynch, 2019). Problems arise, however, in linking satellite-based and ground-based observations. Specifically, satellite-based measurements of the ash mass transported in volcanic clouds typically account for ≤2% of the total deposit mass (e.g., Rose et al., 2001), much less than the estimates of unmapped ash.

Operational volcanic ash dispersion and transport models (VATDMs) used for ash forecasts commonly assume that only 5% of the total erupted mass is transported in far-travelled volcanic clouds (Beckett et al., 2015). This assumption is justified if the tephra mass is dominated by larger grain sizes (> 100 μm), and therefore is deposited in proximal regions. The best-constrained estimates of total grain size distribution (TGSD) are from eruptions in the Americas, where prevailing winds place most of the deposit on land (e.g., Mount St. Helens, USA, 1980; Spurr, USA, 1992; Chaiten, Chile, 2008), or where satellite-based estimates of airborne ash size have been added to ground-based deposits (e.g., Eyjafjallajökull, Iceland; Bonadonna et al., 2011). TGSDs from these eruptions (Fig. 1) show that in well characterized deposits, >50% of the ash comprises particles < 100μm, and up to 10% (or more) of the TGSD comprises particles < 10μm.

A final perspective on far-travelled ash is provided by distal tephrochronology (Ponomareva et al., 2015). The use of tephrochronology as a stratigraphic tool has expanded substantially over the past decades with new methodologies for processing and identifying cryptotephra (e.g., Lowe, 2011; Davies, 2015; Plunkett and Pilcher, 2018). An underlying assumption is that proximal, distal and ultra-distal (cryptotephra) deposits can be linked directly to a specific volcanic eruption (Lowe, 2011; Crocitti et al., 2019). Tephrostratigraphic records can also provide continuous chronologies that are important for understanding patterns of volcanism (Sulpizio et al., 2014; Ponomareva et al., 2015), and preserve data critical for assessing the long-term environmental impacts of volcanic eruptions (e.g., Long et al., 2011).

Together, eyewitness accounts, mapped volcanic deposits, ash transported in volcanic clouds, and ash deposited as cryptotephra should provide a complete record of ash impacts. That these observations are not routinely combined reflects both gaps between disciplines and challenges in reconciling different data types and sources of error. Mapped deposits are typically accurate to ~1-0.1 cm thickness if visited immediately after an eruption. Thin deposits, however, are easily remobilized by wind, water and gravity in the weeks, months and years that follow, adding errors to measurements of

older deposits. Ash clouds can be tracked far beyond mapped deposits, but are limited to ash concentrations >~0.1-0.2 g/m$^2$ (Prata and Lynch, 2019). Cryptotephra data are measured by shard counts that may lie close to this mass-loading limit (Stevenson et al., 2012), although cryptotephra preservation varies with depositional environment, adding uncertainties to estimates of spatial coverage of ash at the time of the eruption (Davies et al. 2007; Lowe, 2011; Watson et al., 2016). Here we examine ways in which these data sources can be combined, with the primary goal of incorporating cryptotephra data into studies of volcanic deposits and the hazards they represent.

**Case studies – well observed eruptions**

To improve our understanding of ash transport and deposition, we first review key elements of well-observed eruptions that, together, highlight the knowns and unknowns of far-travelled volcanic ash.

*Mount St. Helens, USA, 1980*

The climactic eruption of Mount St. Helens on 18 May, 1980, provides an exceptionally detailed record of ash transport. The eruption initiated with a lateral blast to the north, which generated a 30 km high co-blast plume that was subsequently transported east by strong winds in the lower stratosphere (e.g., Sarna-Wojcicki et al., 1981; Eychenne et al., 2015). Explosive activity continued at varying intensities for another 9 hours, during which time the front of the visible ash cloud moved across the states of Washington, Idaho and western Montana, eventually extending into northwestern Wyoming (Fig. 2a). The (uncompacted) tephra deposit was mapped and sampled within days of the eruption (e.g., Sarna-Wojcicki et al., 1981). One interesting feature of the deposit is a pronounced secondary thickening near Ritzville, Washington, more than 300 km from the volcano (Fig. 2b), which has been attributed to premature fallout of fine ash (Carey and Sigurdsson, 1982) and may have contributed to the high proportion of very fine ash in the mapped deposit (Fig. 1). Eyewitness accounts (Scheidegger et al., 1982; Waitt 2015) also record the start of ash fall, which lags the ash cloud front by times that increase with distance from the vent (Fig. 3a).

The deposit thickness data have been used to estimate a total erupted volume of 0.2 km$^3$ (dense rock equivalent, DRE; Sarna-Wojcicki et al., 1981). The outermost (0.5 cm) isopach mapped by Sarna-Wojcicki et al. (1981; Fig. 2a) encloses an area of 4.8 x 10$^4$ km$^2$ and extends 580 km downwind from the source. Exponential extrapolation of these data (Fierstein and Nathenson, 1992) shows that 21% of the deposit mass (= 21% by volume for uniform deposit density) lies outside (is thinner than) the 0.5 cm isopach. Although the assumption of exponential deposit thinning may overestimate the unmapped ash mass if fine ash is deposited prematurely, it is consistent with satellite-based observations of the visible ash cloud well beyond the mapped deposit (Fig. 2a).

The mapped deposit is also displaced to the north compared to the path of the satellite-tracked ash cloud (Fig. 2a). In fact, an interpolated isomass map (Sarna-Wojcicki et al., 1981) extends the northern boundary of the mapped deposit (at 0.001 g/cm$^2$) farther north

toward the Canadian border. Additionally, eyewitness accounts provide evidence for visible ash fall of 1/8$^{th}$ inch (3mm) in Billings Montana (>1000 km east of the volcano and well beyond the mapped limit) by dawn on 19 May (Waitt, 2015). On 19-20 May, ash fall was also observed in SE British Columbia, southern Alberta and SW Saskatchewan (B. Jensen, pers. comm.), and even into NW North Dakota (Waitt, 2015), a distance of almost 1500 km. These eyewitness observations thus document visible ash fall well to the north and east of both the mapped deposit and the visible plume trajectory. At the same time, eyewitness accounts illustrate the hazards associated with even small amounts of volcanic ash, including school closures in Missoula (for one week) and Billings, visibility problems in North Dakota and an aircraft encounter with the ash cloud on 20 May in Utah (south of Idaho; Guffanti et al., 2009).

The spatial extent of ash fall may reflect the exceptionally fine average grain size of this deposit, which derives at least in part from the initial lateral blast (Eychenne et al., 2015; Cashman and Rust, 2016; Fig. 1). Moreover, although the grain size distribution fines with distance from the vent, it stabilizes beyond ~ 300 km, when most (~90%) of the deposit comprises very fine ash (<63 μm; Fig. 3b). Grain size stabilization over similar distances was observed in the deposit from the 2008 eruption of Chaiten, Chile (Durant et al., 2012). Additional information about ash size comes from direct sampling of airborne ash. For example, samples obtained from the stratosphere over Montana on May 19 (Farlow et al., 1981) were 0.1 - 32 μm in size, and suggest that very small ash particles may travel long distances, and remain suspended in the atmosphere for days.

*Mount Pinatubo, Philippines, 1991*

The eruption of Mount Pinatubo initiated with a series of subplinian eruptions from 12-14 June and culminated on 15 June 1991 in a large Plinian eruption with numerous associated pyroclastic density currents (Newhall and Punongbayan, 1996). The main phase of the eruption produced a large umbrella cloud that spread ~200 km upwind, although tephra was dispersed downwind (to the west) and deposited primarily in the South China Sea (Fig. 4a). Although there is no secondary thickness maximum, the deposit thickness is approximately constant along the dispersion axis at ~ 350-550 km from the vent (Fig. 4b). Mapped deposits yield a total erupted mass of 6000 Mt (Wiesner et al., 2004) and, when extrapolated exponentially, suggest that 12% of the mass erupted was deposited beyond the 0.4 cm isopach at 768 km downwind (the most distal grain size sample), and that ~5% of the total mass was deposited beyond the outermost (0.1 cm) isopach, which extends 1000 km downwind.

Airborne ash was mapped by satellite over 1000s of kms (Fig. 5a). The total mass of the maximum measured airborne ash mass from satellite data, however, was 50 Mt (Guo et al. 2004), or <1% of the total mass erupted, and only 17% of the unmapped ash mass. In part, the low airborne ash estimates reflect the high particle load of the proximal ash cloud, which made it opaque to infrared sensors. Satellite observations also documented significant total ice mass (80 Mt) within the volcanic cloud. Ash and ice masses later declined at similar rates, suggesting that ash particles may have acted as an ice nucleator, and that ice-ash aggregates may have both masked ash particles in the plume and

enhanced sedimentation of very fine ash. Ash sedimentation from the volcanic clouds occurred over days, long past the end of the ~9-hour eruption and to distances >4000 km, well beyond the mapped deposit extent of ~1000 km. By three days after the end of the eruption, <10 Mt fine ash remained in the cloud (Guo et al., 2004), which represents ~0.2% of the total erupted mass, but almost 20% of the maximum measured airborne ash mass. From a hazard perspective, it is important to note that 12 damaging ash cloud-aircraft encounters occurred between 700 and 1740 km from the volcano (well beyond the mapped ash deposit), and when the ash cloud was 12-24 hours old (Casadevall et al. 1996).

Ash size distributions are reported for sediment cores to 768 km, where the deposit is 4 mm thick (Wiesner et al., 2004; Fig. 5b). As seen at Mount St. Helens, the grain size distribution stabilizes in the distal deposits (>~500 km) when most of the ash is <63 μm in size. The mean effective radius of the airborne ash was 6-9 μm (Guo et al., 2004); for a log normal size distribution, this equates to a median diameter (by mass) of ~ 20 μm and a maximum ($95^{th}$ percentile) of ~ 63 μm (Stevenson et al., 2015), in reasonable agreement with the distal ash grain size distributions shown in Figure 5b. By particle number, however, this effective radius equates to a median particle diameter of <5 μm (Stevenson et al., 2015), which may be important for ice nucleation.

Within a few months, ash had accumulated just above the tropopause, where it persisted ≥ 10 months. Small ash particles (2-10 μm) of Pinatubo composition were found in 1993 and 1994 south polar snow layers ~12,000 km from the volcano (Cole-Dai et al., 1997), suggesting that although thin ash (and cryptotephra) layers can form syn-eruptively (within a few days) to 1000s of km from the source vent, transfer of ash particles from low latitudes to polar regions may take months to years.

*Eyjafjallajökull 2010*

The ash cloud produced by the Eyjafjallajökull eruption of 2010 was exceptionally well characterized because of the severe financial and personal impact of airspace closure during this event (e.g., Ulfarsson and Unger, 2011). Despite the attention from the volcanology, remote sensing and atmospheric science communities, however, fundamental questions remain with regard to the nature of the erupted material, its transport and deposition.

Ground-based studies in Iceland provide isopach maps for individual eruptive phases (Bonadonna et al., 2011), as well as a cumulative thickness plot for the entire eruption, which lasted from mid-April to late May (Gudmundsson et al., 2012). Isopachs for the total deposit were mapped on land to thicknesses of 0.01 cm and indicate a total volume of 140 ± 20 x $10^6$ $m^3$. Extrapolations of ash deposition beyond Iceland, including the "minor dusting" of ash in northern Europe (assumed thickness 0.1 μm), suggest a total erupted tephra volume of ~270 ± 70 x $10^6$ $m^3$, which is equivalent to 378 Mt (tephra density = 1400 kg/$m^3$). By this estimate, almost 50% of the tephra mass was deposited outside of Iceland, with ~ 10 Mt ash likely transported >600-700 km but less than 1% of which would have reached mainland Europe (Gudmundsson et al., 2012). The total mass

of airborne ash (particle size 2.8-28 μm diameter) has been estimated at ~ 8 Mt (Stohl et al., 2011). Gudmundsson et al. (2012) argue that this represents slightly more than 10% of the total mass of very fine ash (<28 μm) deposited outside of Iceland, but up to 25% of the fine ash for the mid-April period of observation.

Far-travelled ash from the 2010 eruptions was examined by Stevenson et al. (2012), who collected ash data from both rain gauges and PM10 monitors (which measure the atmospheric load of particles <10 μm). Figure 6 shows the data collection sites, together with the observed distribution of airborne ash (daily ash loadings >0.2 g/m$^2$; Gudmundsson et al., 2012) for the periods of explosive activity (14-17 April; 5-18 May). Proximal (to ~100 km) samples of the early (phreatomagmatic) phase of the eruption have high (20-25%) mass fractions of very small particles (<10 μm) and a median < 32μm (Gislason et al., 2011). Bulk ash samples collected in the Faroes, however, have a modal size of 40 μm, while samples from rainwater gauges in British Isles and Norway have a modal maximum size (maximum measured diameter of all grains >10 μm) of 25 and 48 μm, respectively; in all three locations, the maximum particle size is ~100 μm (Stevenson et al., 2012). Grain counts in rain gauge samples would translate to 8-218 shards/cm$^2$, if measured as cryptotephra (Stevenson et al., 2012). These relatively large far-travelled particles are vesicular and/or highly anisotropic, characteristics that decrease the settling velocity and increase the effective transport distance (Beckett et al., 2015; Saxby et al., 2018).

*Askja 1875*

The deposit produced by the 1875 eruption of Askja volcano, Iceland, provides a bridge between mapped deposits and observations of ultradistal ash fall, as illustrated by Carey et al. (2010). The 28-29 March eruption produced strong phreatoplinian and Plinian phases that together lasted ~17 hours, ejected ~1000 Mt magma and ultimately prompted a migration of eastern Icelanders to Canada. The Askja deposit was originally mapped by Sparks et al. (1981), who identified both phreatomagmatic and magmatic phases of the eruption. From these field data, they constructed an isopach map to ~100 km (the greatest extent of the subaerial deposit) and 1 cm thickness, and estimated a total grain size distribution (Fig. 1). Extrapolation of this isopach map suggests about 15% missing volume (beyond 1 cm; Fierstein and Nathenson, 1992).

Eyewitness accounts were collected and interpolated by Mohn (1877) to construct isochrones for the beginning of ash fall across the North Atlantic and Scandinavia (Fig. 7a). These data show that ash fall on the east coast of Iceland (80-100 km from Askja) started at 7 am (GMT) on 29 March, reached western Norway at 2100-2200 on the same day (2200-2300, local time in Scandanavia) and extended to Stockholm, Sweden, by 10am (local time) on 30 March. Selected accounts reported in Thorarinsson (1981) state that “fine, grayish sand fell with the rain” [western Norway, ~1200 km from Askja], “dust fell which caused unaccountable pain in the eyes” [Norway-Sweden border], and “hot-bed frames so closely covered with a grey dust that they scarcely admitted any light” [Stockholm, ~1900 km]. Carey et al. (2010) used ash thicknesses inferred from these accounts and known cryptotephra sites to extend the proximal isopachs across the North

Atlantic to Scandanavia, including designation of a "visual trace" ($10^{-4}$ cm, a limit that Watt et al. (2012) equate with a "pale dusting") and a "detectable limit" of $10^{-5}$ cm (cryptotephra; Fig. 7b). Importantly, these expanded isopachs increase the total erupted volume of the magmatic phase from 0.32 to 1.37 $km^3$, and estimates of the extrapolated ash proportion deposited beyond Iceland from 15% to 66%. These data also provide insight into the TGSD shown in Figure 1. As plotted, it appears to be unusually coarse-grained. If viewed as representative of only 44% of the total mass, however, the TGSD can be interpreted as reflecting an unusually coarse proximal deposit that is missing most of the very fine ash fraction. Indeed, particle size data provided by Stevenson et al. (2015) for a sample collected 1500 km from source yields a median size of 55μm and a $95^{th}$ percentile measurement of 115μm.

Here we extend use of the cryptotephra record by including sites discovered since 2010. To translate shard counts to an estimated (or pseudo-) thickness, we first convert reported shard counts per volume (S/V) to shards/area (S/A) by dividing S/V by the sample depth interval. S/A data are then converted to pseudo-thickness using the diameter of a volume-equivalent sphere based on the shard size. Although the actual volume of each (non-spherical) shard will be less, this volume approximates the (imperfect) packing of the deposit. Because of the paucity of size data, we assume a diameter of 100 μm close to the main dispersion axis (e.g., Lacasse, 2001; Stevenson et al., 2015) and a diameter of 40 μm in the most distal deposits (based on images in Stivrins et al., 2016; Wulf et al., 2016).

Askja cryptotephra deposits found in central Norway and Sweden have high shard counts (~2000-3000 shards/$cm^3$; Supplementary Material) that translate to pseudothicknesses ~10-20 μm (Fig. 7b). Lower shard counts (≤ 100/$cm^3$) and smaller ash sizes in northern Norway, Germany and Latvia yield thicknesses of <1 μm toward the outer limits of the depositional area. These data agree well with the thickness estimates of Carey et al. (2010), with a few modifications. First, although the Klocka Bog sample (KB in Figure 7b) lies fairly close to the 1 mm isopach of Carey et al. (2010), the cryptotephra data suggest a thickness of only ~ 10 μm. This discrepancy could reflect problems in deposit preservation. Alternatively, it may record over-thickening of deposits on the windward side of the mountains that line the Norwegian coast. In fact, such over-thickening has been suggested for the older Vedde ash deposit (Mangerud et al., 1984; Saxby, this volume) and may be a general feature of Icelandic tephra deposition in Norway. Second, our interpretation of the cryptotephra data suggest that the $10^{-4}$ cm (0.1 μm) isopach may encompass a smaller area than currently mapped, and that the cryptotephra record of ash deposition ($10^{-5}$ cm, or 0.01 μm isopach) may extend farther to the east (e.g., Stivrins et al., 2016).

**Implications for understanding past eruptions and future ash hazards**

Although the 1875 Askja eruption was large (VEI ~ 5), much larger Icelandic eruptions appear in the cryptotephra record of northern Europe (e.g., the Vedde ash; Saxby et al., this volume). Recent reviews also provide evidence that very large eruptions (~VEI 7) in western North America may produce cryptotephra deposits in eastern North America,

Europe and Greenland (e.g., Jensen et al., 2014; Bourne et al., 2016; Watson et al., 2017; Plunkett and Pilcher, 2018). What can these cryptotephra records tell us about ash hazards and impacts that accompanied these events?

*The 860 CE White River Ash, USA*

To answer this question, we briefly examine the deposit comprising the White River Ash (east; WRAe), which was produced by a very large eruption of the Bona-Churchill massif in SE Alaska. Athapaskan oral traditions of an apparent volcanic eruption have been connected to this event, and the resulting environmental disruption inferred to have displaced and dispersed local populations to as far as the American southwest (Moodie et al., 1992; Hare et al. 2004). Isopachs have been mapped by Lerbekmo (2008) to 1 mm at ~1000 km (Fig. 8a), and suggest a deposit volume of 47 $km^3$ (22.5 $km^3$ dense rock equivalent).

WRAe cryptotephra has been identified in SE Alaska and NE North America, as well as in the UK and northern Europe, and in Greenland ice cores (Jensen et al., 2014; Fig. 6a). Unfortunately, data on shard counts and ash size are available only for the Nordan's Pond Bog site in Newfoundland (Pyne-O'Donnell et al., 2012). Here observed shard counts of ~650/5$cm^3$ and a mean ash size of ~40 μm yield a pseudo-thickness of ~0.2 μm, equivalent to the outer limit of the 1875 Askja isopachs in Europe. Interestingly, this estimated pseudo-thickness lies on an exponential extrapolation of thickness data from the more proximal mapped deposits (Fig. 6b). Shown for comparison are thickness-distance estimates for the much smaller (<2 $km^3$) 1875 Askja deposit (Fig. 5a). WRAe ash particles in Greenland ice cores are <10 μm in size, similar to the Pinatubo ash particles preserved in Antarctic ice cores.

*Combining records of ash behavior during explosive eruptions*

We have shown that combining the scientific approaches of physical volcanology, remote sensing and tephrochronology can improve understanding of ash hazards and impact, as well as aid understanding of fundamental processes of volcanic ash transport and deposition. Yet syntheses of data from these different sources are rare. Attempts to reconcile mapped deposits with satellite-based observations show reasonable spatial correlations between ash clouds and resulting deposits to 100s of km, but fail to account for extrapolated estimates of unmapped ash at greater distances. A partial explanation for this discrepancy may be that IR-based retrieval methods are limited to ash sizes of 1-32 μm diameter (Prata and Lynch, 2019), and therefore may be missing ash mass in both smaller and larger size fractions (Stevenson et al., 2015). Also difficult to reconcile are the small ash sizes inferred from satellite retrievals, and used as input for most ash dispersion and transport models, compared with the large size reported for far-traveled ash particles (Lacasse, 2001; Stevenson et al., 2015; Cashman and Rust, 2016). Large ash particles are also more anisotropic, and often more vesicular, than modeled particles (e.g., Saxby et al., 2018). The application of cryptotephra data to volcanological studies is rare, although the Askja example (e.g., Carey et al., 2010; Fig. 7b) shows the potential of using cryptotephra data to estimate eruption volumes where most of the ash transport and

deposition occurs over the ocean. We suggest that these data can also help to reconcile mapped deposits and ash cloud data and, when combined with eyewitness accounts, can improve volcanic hazard assessments.

Distal eyewitness accounts from the Mount St. Helens eruption demonstrate that even light ash fall can cause immediate problems related to transport, and that "ash mists" caused by far-traveled very fine ash can persist for days (Waitt, 2015). Evidence for ash-and-aircraft encounters at great distances, and days after, major eruptions (Casadevall et al., 1996; Guffanti et al., 2009) shows that equivalent low concentration ash loads in the atmosphere can severely impact aviation, and cause long-term health problems (Newnham et al., 2010). Although atmospheric ash loading is impossible to calculate for past deposits, direct comparison of cryptotephra data and eyewitness accounts of ash fall during the 1875 Askja eruption suggests that shard counts of 1000s/cm$^2$ (pseudo-thickness ~10s of microns) are visible and produce measurable impacts during the periods of primary ash fall. Observations from the Eyjafjallajökull eruption further show that primary deposition of ultra-distal ash at concentrations equivalent to 100s of shards/cm$^2$ was sufficiently high for modern methods of satellite-based detection. Small distal ash particles are also prone to both immediate (e.g., Waitt, 2015) and long-term (Wilson et al., 2011; Liu et al., 2014) resuspension and transport by wind. Together these datasets suggest that including data on far-travelled ash could substantially improve volcanological estimates of ash impacts caused by future eruptions and improve constraints on source parameters for volcanic ash dispersion and transport models (VATDMs).

*Improving source parameters for VATDMs*

Model protocols for forecasting ash clouds vary, but many ash dispersion models, including the operational forecasts of the London and Toulouse Volcanic Ash Advisory Centers (VAACs), assume that only 5% of the total erupted mass (the "distal fine ash fraction"; DFAF) comprises far-travelled volcanic clouds and is therefore of interest to the forecaster. In fact, Gouhier et al. (2019) argue that even 5% is too high for most eruptions, and suggest that satellite-based observations indicate DFAF for Plinian eruptions of ≤0.9%. The largest eruption in their data set is Pinatubo 1991, where the deposit is mapped to ~1000 km from source (an area of 4 x $10^5$ km$^2$). We estimate from Wiesner et al. (2004) data that ~5% of the mass lies beyond the 0.1 cm isopach; moreover, the suggested mass limit of 0.9% lies beyond the (extrapolated) 0.2 mm isopach (area = 8 x $10^5$ km$^2$), well beyond both the mappable limit and the airspace including most ash encounters (Casadevall et al., 1996). Indeed, our analysis suggests that for many eruptions, modeling only 5% of the mass may severely underestimate ash mass loading in far-travelled volcanic clouds, and that as much as 10-20% of the deposited ash mass may lie beyond the 1 cm isopach (the mapped limit for most older deposits), and that this value may exceed 50% when the extent of subaerial deposits is limited (as is often the case in Iceland).

Improving constraints on far-traveled ash requires better documentation of the grain size and thickness of ash deposits in distal and ultra-distal sites. For deposits of past very large

eruptions, distal data are often insufficient for isopach construction, and thus for use in traditional log thickness vs. √area plots used to determine the erupted volume. Plots of log thickness vs. distance, however, can be used to construct thickness envelopes that provide important information on the area impacted by that event (e.g., Mathews et al., 2012; Engwell et al., 2014). Additionally, grain size and shape data from ultradistal (>1000 km) sites can be combined with ash dispersion models to constrain eruption column height (mass eruption rate) and wind conditions (Saxby et al., this volume), and to improve the use of ice cores for paleoclimate studies (Dunbar et al., 2017). Critically, however, most deposit studies lack information on the abundance of ultrafine (< 10 μm) ash particles because of measurement difficulties (Bagheri and Bonadonna, 2016), although this size class may comprise ≤10% of mapped deposits (Fig. 1) and the bulk of many ice cores samples (Jensen et al., 2014.

**Summary**

We have used data from well-characterized recent eruptions to relate mapped deposits on the ground to eyewitness accounts of primary ash fall and short-term impacts, satellite-based observations of ash in the air and cryptotephra records of past eruptions. Together these case studies highlight knowledge gaps between models of tephra deposition in proximal environments and conditions allowing ash transport for 100s to 1000s of km. Notable are the mismatches between the total mass erupted (extrapolated from mapped deposits), the mass within the mapped region (often 80-90% of the total, although sometimes <70%), satellite-based estimates of airborne ash mass (typically 1-2% of the total) and the initial ash mass input into VATDMs (5% of total). Reconciling these datasets is critical for accurate ash forecasts during future large eruptions and assessment of syn- and post-eruption ash impacts.

Cryptotephra data have the potential to improve constraints on the abundance and physical characteristics of the missing ash. Thin (or trace) deposits preserved in sediments, lakes and bogs can also provide key information on more frequent smaller eruptions, the deposits of which are poorly preserved in the terrestrial geological record (e.g., McNamara et al. 2018). Incorporating distal tephra data into volcanological studies requires not only chemical fingerprinting of constituent glass shards but also information on mass and/or particle concentrations. Practically, this means making multiple measurements per site (e.g., Watkins et al., 2016) and supplementing shard counts per sample volume with measurements of particle size and shape (e.g., Saxby et al., this volume). Perhaps surprisingly, where these data are available for large eruptions, they appear to confirm assumptions of exponential thinning over very great distances. Missing from all records, however, is documentation of very small (<20-25 μm) ash particles, which are not often analysed but are known to reside in the atmosphere for at least months after large eruptions (e.g., Cashman and Rust, 2016).

**Acknowledgements** The authors would like to acknowledge informative discussions with Jen Saxby and Hannah Buckland (U.Bristol), Frances Beckett (MetOffice), Stefan Waastgard and Simon Larsson (U.Stockholm), David Lowe (U.Waikato), Britta Jensen (U. Alberta), Siwan Davies (U.Swansea) and John Westgate (U.Toronto). We would also

like to thank three anonymous reviewers and R. Sulpizio for helpful suggestions. KVC was supported by a Royal Society Wolfson Fellowship and an AXA Professorship.

**References**


Bagheri, G. & Bonadonna, C. (2016a) Aerodynamics of volcanic particles: characterization of size, shape, and settling velocity, *Volcanic Ash.* Elsevier, 39-52.

Beckett, F *et al.* (2015) Sensitivity of dispersion model forecasts of volcanic ash clouds to the physical characteristics of the particles. *Journal of Geophysical Research-Atmospheres*, 120(22).

Bergman, J. *et al.* (2004) Holocene tephra horizons at Klocka Bog, west-central Sweden: aspects of reproducibility in subarctic peat deposits. *Journal of Quaternary Science*, 19(3), 241-249.

Bonadonna, C. & Costa, A. (2012) Estimating the volume of tephra deposits: A new simple strategy. *Geology*, 40(5), 415-418.

Bonadonna, C. *et al.* (2011) Tephra sedimentation during the 2010 Eyjafjallajokull eruption (Iceland) from deposit, radar, and satellite observations. *Journal of Geophysical Research-Solid Earth*, 116.

Bourne, A. *et al.* (2016) Underestimated risks of recurrent long-range ash dispersal from northern Pacific Arc volcanoes. *Scientific Reports*, 6.

Carey, R. *et al.*(2010) Tephra dispersal and eruption dynamics of wet and dry phases of the 1875 eruption of Askja Volcano, Iceland. *Bulletin of Volcanology*, 72(3), 259-278.

Carey, S. N. & Sigurdsson, H. (1982) Influence of Particle Aggregation on Deposition of Distal Tephra from the May 18, 1980, Eruption of Mount St-Helens Volcano. *Journal of Geophysical Research*, 87(Nb8), 7061-7072.

Casadevall, T. J. *et al.* (1996) The 1991 Pinatubo eruptions and their effects on aircraft operations. *Fire and Mud: eruptions and lahars of Mount Pinatubo, Philippines*, 625-636.

Cashman, K. & Rust, A. (2016) Volcanic ash: generation and spatial variations. *Volcanic Ash.* Elsevier, 5-22.

Cioni R. *et al.* (2003) Assessing pyroclastic fall hazard through field data and numerical simulations: Examples from Vesuvius. *Journal of Geophysical Research-Solid Earth*, 108.

Cole-Dai, J. *et al.* (1997) Quantifying the Pinatubo volcanic signal in south polar snow. *Geophysical Research Letters*, 24(21), 2679-2682.

Crocitti, M. *et al.* (in press) On ash dispersal from moderately explosive volcanic eruptions: Examples from Holocene and Late Pleistocene eruptions of Italian volcanoes. *Journal of Volcanology and Geothermal Research.*

Davies, S. (2015) Cryptotephras: the revolution in correlation and precision dating. *Journal of Quaternary Science*, 30(2), 114-130.

Davies, S. *et al.* (2007) Cryptotephra sedimentation processes within two lacustrine sequences from west central Sweden. *Holocene*, 17(3), 319-330.

Dunbar, N. *et al.* (2017) New Zealand supereruption provides time marker for the Last Glacial Maximum in Antarctica. *Scientific Reports*, 7.

Durant, A. *et al.* (2012) Long-range volcanic ash transport and fallout during the 2008 eruption of Chaiten volcano, Chile. *Physics and Chemistry of the Earth*, 45-46, 50-64.

Engwell, S. L. *et al.* (2014) Physical characteristics of tephra layers in the deep sea realm: the Campanian Ignimbrite eruption. *Marine Tephrochronology*, 398, 47-64.
Eychenne, J. *et al.* (2015) Impact of the lateral blast on the spatial pattern and grain size characteristics of the 18 May 1980 Mount St. Helens fallout deposit. *Journal of Geophysical Research-Solid Earth*, 120(9), 6018-6038.
Eychenne, J. *et al.* (2017) Distal Enhanced Sedimentation From Volcanic Plumes: Insights From the Secondary Mass Maxima in the 1992 Mount Spurr Fallout Deposits. *Journal of Geophysical Research-Solid Earth*, 122(10), 7679-7697.
Farlow, N. H. *et al.* (1981) Size distributions and mineralogy of ash particles in the stratosphere from eruptions of Mount St-Helens. *Science*, 211(4484), 832-834.
Fierstein, J. & Nathenson, M. (1992) Another look at the calculation of fallout tephra volumes. *Bulletin of Volcanology*, 54(2), 156-167.
Gislason, S. R. *et al.* (2011) Characterization of Eyjafjallajokull volcanic ash particles and a protocol for rapid risk assessment. *Proceedings of the National Academy of Sciences of the United States of America*, 108(18), 7307-7312.
Gouhier, M., *et al.* (2019) Low efficiency of large volcanic eruptions in transporting very fine ash into the atmosphere. *Scientific Reports*, 9.
Gudmundsson, M. *et al.* (2012) Ash generation and distribution from the April-May 2010 eruption of Eyjafjallajokull, Iceland. *Scientific Reports*, 2.
Guffanti, M. *et al.* (2009) Volcanic hazards to airports. *Natural Hazards*, 51(2), 287-302.
Guo, S. *et al.* (2004) Particles in the great Pinatubo volcanic cloud of June 1991: The role of ice. *Geochemistry Geophysics Geosystems*, 5.
Hare, P. *et al.* (2004) Ethnographic and archaeological investigations of alpine ice patches in southwest Yukon, Canada. *Arctic*, 57(3), 260-272.
Jenkins, S. *et al.* (2015) Volcanic ash fall hazard and risk. *Global Volcanic Hazards and Risk*, 173-222.
Jensen, B. *et al.* (2014) Transatlantic distribution of the Alaskan White River Ash. *Geology*, 42(10), 875-878.
Lacasse, C. (2001) Influence of climate variability on the atmospheric transport of Icelandic tephra in the subpolar North Atlantic. *Global and Planetary Change* 29:31-55.
Larsson, W. (1937) Vulkanische Asche vom Ausbruch des Chilenischen Vulkans Quizapú (1932) in Argentina gesammelt. *Bulletin Geological Institution of Uppsala*, 26, 27-52.
Lawson, I. *et al.* (2012) The spatial distribution of Holocene cryptotephras in north-west Europe since 7 ka: implications for understanding ash fall events from Icelandic eruptions. *Quaternary Science Reviews*, 41, 57-66.
Lerbekmo, J. (2008) The White River Ash: Largest Holocene Plinian tephra. *Canadian Journal of Earth Sciences*, 45(6), 693-700.
Long, C. *et al.* (2011) The effects of fire and tephra deposition on forest vegetation in the Central Cascades, Oregon. *Quaternary Research*, 75(1), 151-158.
Lowe, D. (2011) Tephrochronology and its application: A review. *Quaternary Geochronology*, 6(2), 107-153.
Mackie, S. *et al.* (2016) *Volcanic ash: hazard observation.* Elsevier.

Mangerud, J. *et al.* (1984) A Younger Dryas ash bed in western Norway, and its possible correlations with tephra in cores from the Norwegian Sea and the North-Atlantic. *Quaternary Research*, 21(1), 85-104.

Matthews, N. E. *et al.* (2012) Ultra-distal tephra deposits from super-eruptions: Examples from Toba, Indonesia and Taupo Volcanic Zone, New Zealand. *Quaternary International*, 258, 54-79.

McGimsey, R. G. *et al.* (2001) Areal distribution, thickness, mass, volume, and grain size of tephra-fall deposits from the 1992 eruptions of Crater Peak vent, Mt. Spurr volcano, Alaska. *U.S. Geological Survey Open-File Report* 01-370.

Mohn M. (1877) Askeregnen den 29de-30te Marts 1875. Forhandlinger i Videnskaps-selskabet i Christiania aar 1877(10): 1-12.

Moodie, D. *et al.* (1992) Northern Athapaskan oral traditions and the White River Volcano. *Ethnohistory*, 39(2), 148-171.

Newnham, R. *et al.* (2010) An investigation into long-distance health impacts of the 1996 eruption of Mt Ruapehu, New Zealand. *Atmospheric Environment*, 44(12), 1568-1578.

Plunkett, G. & Pilcher, J. (2018) Defining the potential source region of volcanic ash in northwest Europe during the Mid- to Late Holocene. *Earth-Science Reviews*, 179, 20-37.

Ponomareva, V. *et al.* (2015) Tephra without Borders: Far-Reaching Clues into Past Explosive Eruptions. *Frontiers in Earth Science*, 3.

Prata, F. & Lynch, M. (2019) Passive Earth Observations of Volcanic Clouds in the Atmosphere. *Atmosphere*, 10(4).

Pyle, D. M. (1989) The Thickness, Volume and Grainsize of Tephra Fall Deposits. *Bulletin of Volcanology*, 51(1), 1-15.

Pyne-O'Donnell, S. *et al.* (2012) High-precision ultra-distal Holocene tephrochronology in North America. *Quaternary Science Reviews*, 52, 6-11.

Riehle, J. *et al.* (1994) Unmanned aerial sampling of a volcanic ash cloud. *Eos, Transactions American Geophysical Union*, 75(12), 137-138.

Rose, W. *et al.* (2001) Observations of volcanic clouds in their first few days of atmospheric residence: The 1992 eruptions of Crater Peak, Mount Spurr volcano, Alaska. *Journal of Geology*, 109(6), 677-694.

Rust, A. C. & Cashman, K. V. (2011) Permeability controls on expansion and size distributions of pyroclasts. *Journal of Geophysical Research-Solid Earth*, 116.

Sapper, K. (1904) *Die vulcanischen Ereignisse in Mittelamerika im Jahre 1902*.

Sarna-Wojcicki, A. M. *et al.* (1981) Areal distribution, thickness, mass, volume, and grain size of air-fall ash from the six major eruptions of 1980.

Saxby, J. *et al.* (2018) The impact of particle shape on fall velocity: Implications for volcanic ash dispersion modelling. *Journal of Volcanology and Geothermal Research*, 362, 32-48.

Scheidegger, K. F. *et al.* (1982) Compositional heterogeneity of tephras from the 1980 eruptions of Mount St Helens. *Journal of Geophysical Research*, 87(NB13), 861-881.

Sparks, R. S. J. *et al.* (1981) The Pyroclastic Deposits of the 1875 Eruption of Askja, Iceland. *Philosophical Transactions of the Royal Society of London Series a-Mathematical Physical and Engineering Sciences*, 299(1447), 241-&.

Stevenson, J. *et al.* (2012) Distal deposition of tephra from the Eyjafjallajokull 2010 summit eruption. *Journal of Geophysical Research-Solid Earth*, 117.

Stevenson, J. *et al.* (2015) Big grains go far: reconciling tephrochronology with atmospheric measurements of volcanic ash. *Atmospheric Measurement Techniques Discussions*, 8(1), 65-120.

Stivrins, N. *et al.* (2016) Detection of the Askja AD 1875 cryptotephra in Latvia, Eastern Europe. *Journal of Quaternary Science*, 31(5), 437-441.

Stohl, A. *et al.* (2011) Determination of time- and height-resolved volcanic ash emissions and their use for quantitative ash dispersion modeling: the 2010 Eyjafjallajokull eruption. *Atmospheric Chemistry and Physics*, 11(9), 4333-4351.

Sulpizio *et al.* (2014) Volcanic ash hazard in the Central Mediterranean assessed from geological data. *Bulletin of Volcanology*, 76, 866-874.

Swindles, G. *et al.* (2011) A 7000 yr perspective on volcanic ash clouds affecting northern Europe. *Geology*, 39(9), 887-890.

Swindles, G. T. *et al.* (2013) Volcanic ash clouds affecting Northern Europe: the long view. *Geology Today*, 29(6), 214-217.

Thorarinsson (1981) Greetings from Iceland - Ash-falls and volcanic aerosols in Scandinavia. *Geografiska Annaler Series a-Physical Geography*, 63(3-4), 109-118.

Thorarinsson (1967) *The eruption of Hekla, 1947-1948*, *2*HF Leiftur.

Ulfarsson, G. & Unger, E. (2011) Impacts and Responses of Icelandic Aviation to the 2010 Eyjafjallajokull Volcanic Eruption Case Study. *Transportation Research Record* (2214), 144-151.

Waitt, R. B. (2015) *In the path of destruction: Eyewitness chronicles of Mount St. Helens*. WSU Press, 413 pp.

Watson, E. *et al.* (2016) Do peatlands or lakes provide the most comprehensive distal tephra records? *Quaternary Science Reviews*, 139, 110-128.

Watson, E. *et al.* (2017) Estimating the frequency of volcanic ash clouds over northern Europe. *Earth and Planetary Science Letters*, 460, 41-49.

Watt, S.F.L. *et al.* (2009) Fallout and distribution of volcanic ash over Argentina following the May 2008 explosive eruption of Chaitén, Chile. *Journal of Geophysical Research-Solid Earth*, 114.

Wiesner, M. *et al.* (2004) Grain size, areal thickness distribution and controls on sedimentation of the 1991 Mount Pinatubo tephra layer in the South China Sea. *Bulletin of Volcanology*, 66(3), 226-242.

Wulf, S. *et al.* (2016) Holocene tephrostratigraphy of varved sediment records from Lakes Tiefer See (NE Germany) and Czechowskie (N Poland). *Quaternary Science Reviews*, 132, 1-14.

Figure 1. Total grain size distributions (TGSDs) for well characterized tephra deposits. Data displayed as cumulative plots (mass > a given size), with guidelines plotted for 10µm and 100µm sizes, and for median and 90% values. Data from Sparks et al. (1981; Askja), Rust and Cashman (2016; Mount St. Helens (MSH), Spurr), Bonadonna et al. (2011; Eyjafjallajökull (Eyja)), and Watt et al. (2012; Chaiten).

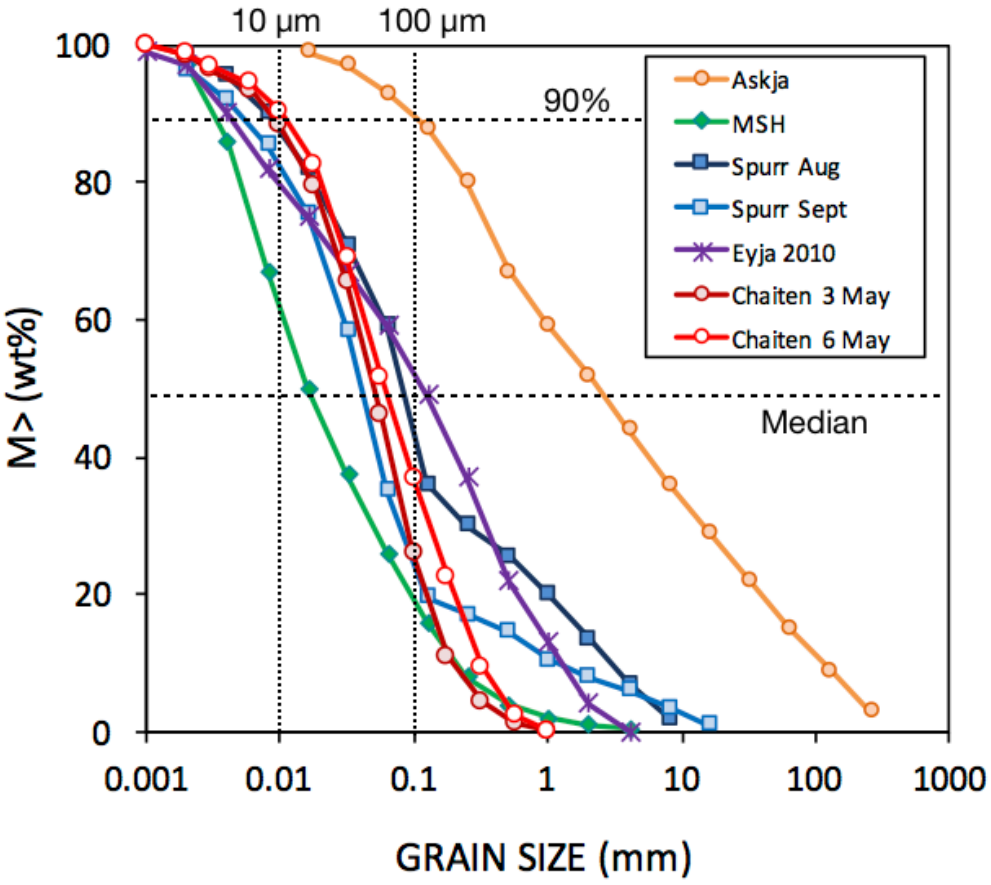

Figure 2. Tephra deposit from the 18 May, 1980, eruption of Mount St. Helens, USA. (a) Map showing movement of the ash cloud front (denoted by local time) and isopach map using uncompacted thickness measurements. (b) Plot of uncompacted deposit thickness with distance along deposit axis. All data from Sarna-Wojcicki et al. (1981), background map made using GeoMapApp (www.geomapapp.org).

Figure 2a

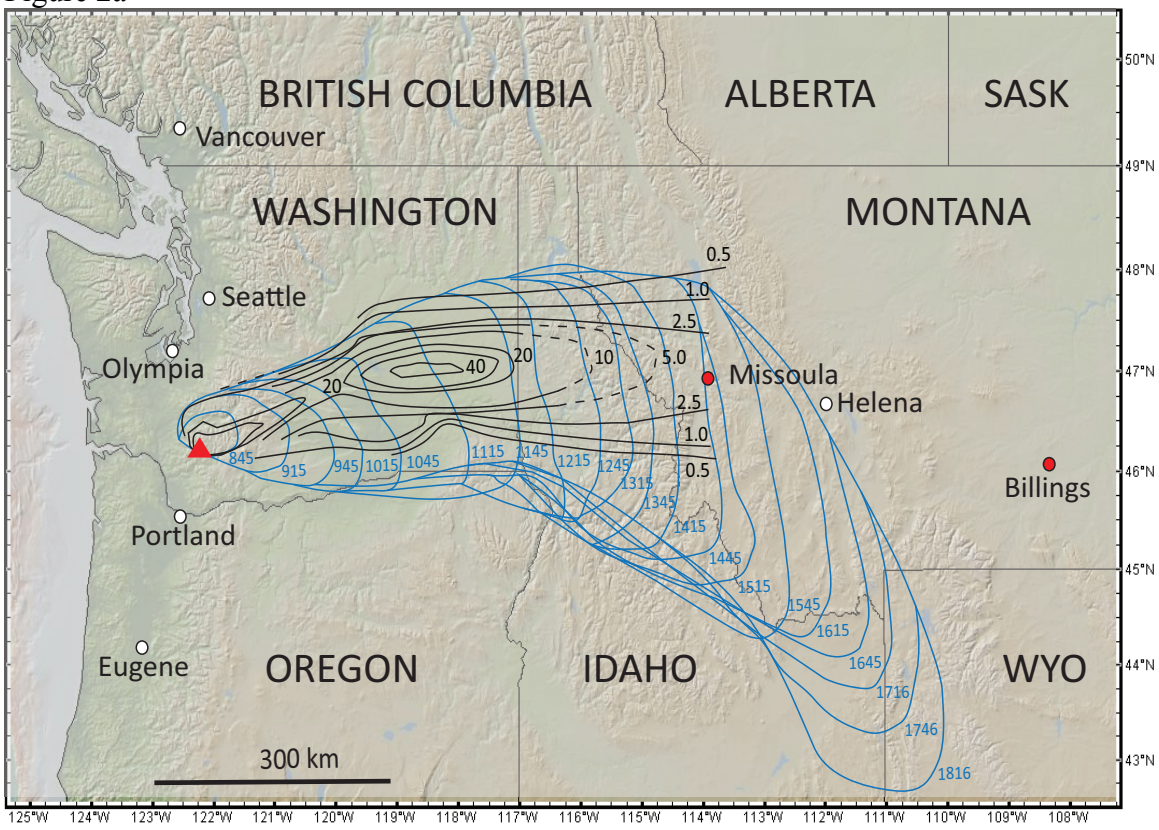

Figure 2b

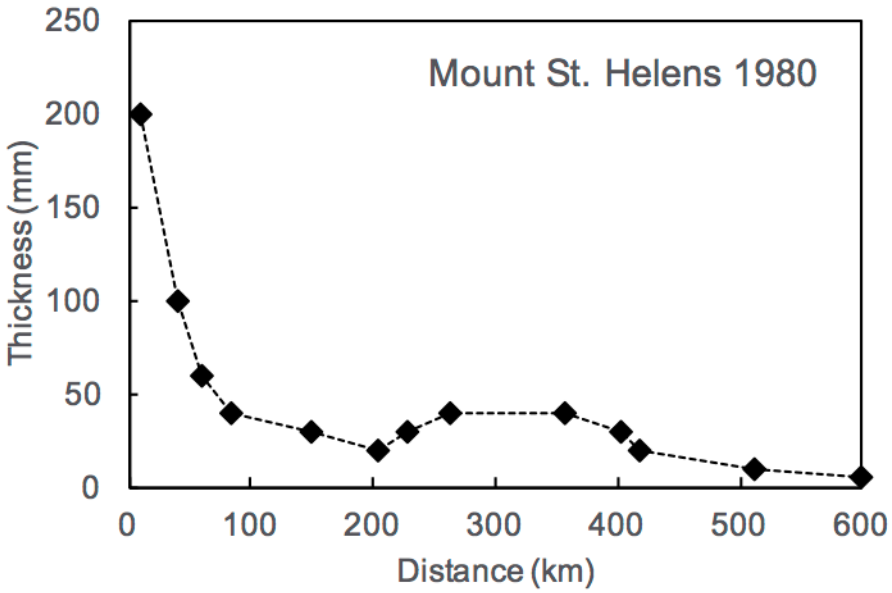
Mount St. Helens 1980
Thickness (mm)
250
200
150
100
50
0
0
100
200
300
400
500
600
Distance (km)

Figure 3. 18 May tephra deposit. (a) Movement (in time) of ash cloud front and observations of first tephra fall on the ground. (b) Deposit grain size distributions as a function of distance along deposit axis, show as sample mass <63 µm (very fine ash), 32 µm (nominal upper limit for satellite detection) and 2 µm (respirable). Data from Eychenne et al. (2015), Waitt (2015).

Figure 3a

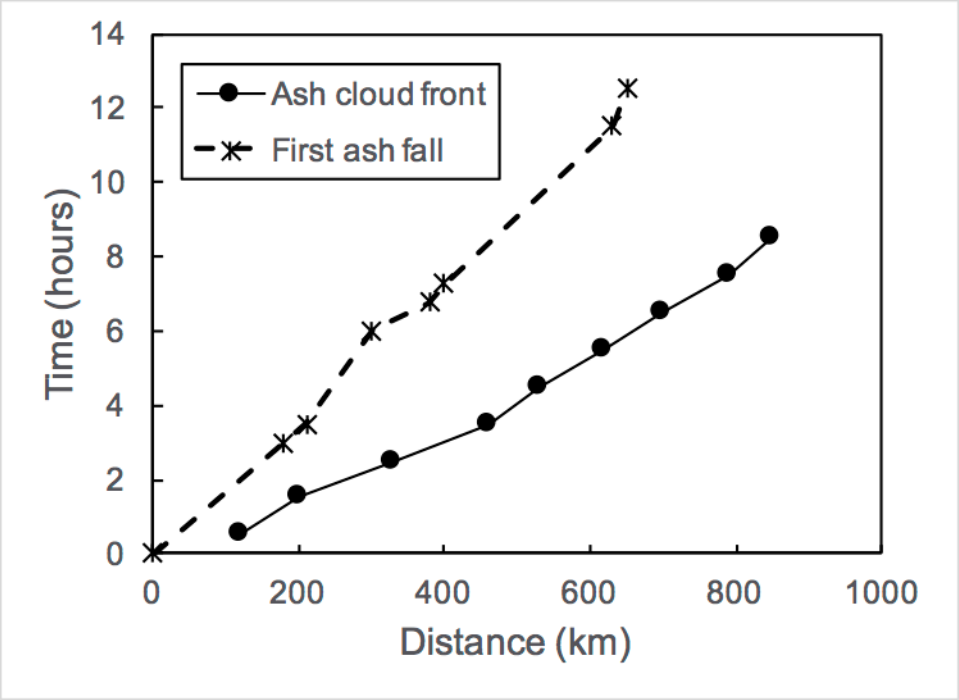

Figure 3b

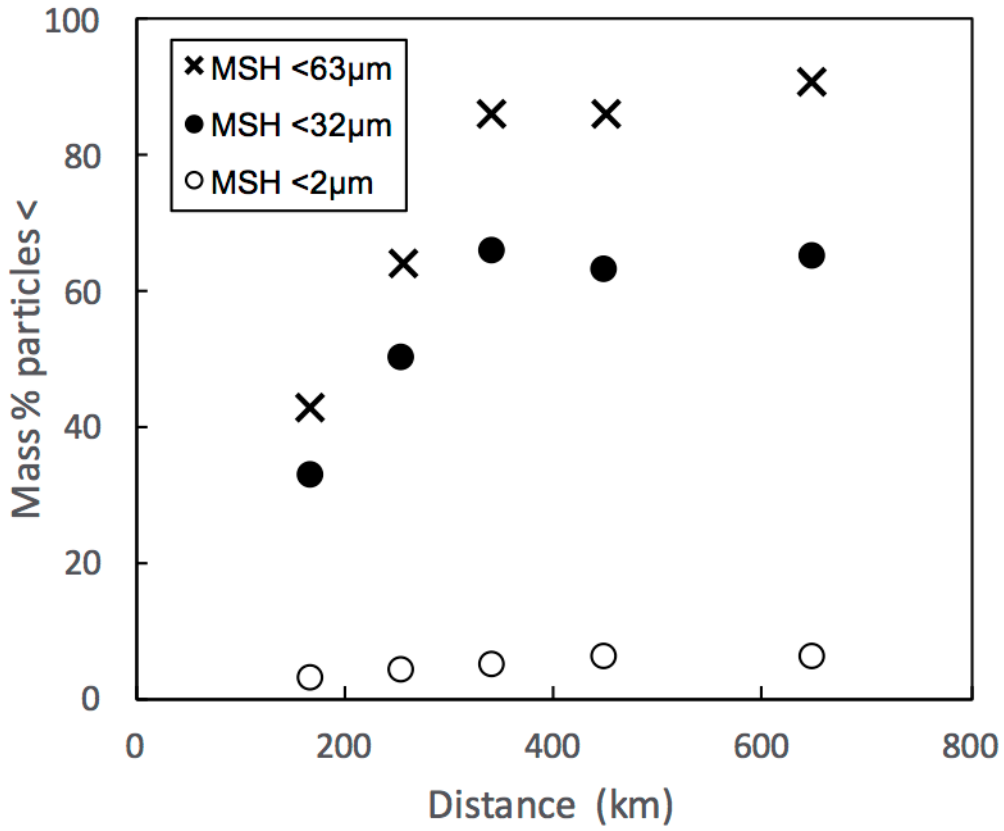
MSH <63μm
MSH <32μm
MSH <2μm
Mass % particles <
100
80
60
40
20
0
0
200
400
600
800
Distance (km)

Figure 4. Tephra deposit from the 15 June, 1991, eruption of Pinatubo, Philippines. (a) Mapped deposit thickness, contours are in mm. (b) Plot of thickness vs. distance along deposit axis. Data from Wiesner et al. (2004), background map made using GeoMapApp (www.geomapapp.org).

Figure 4a

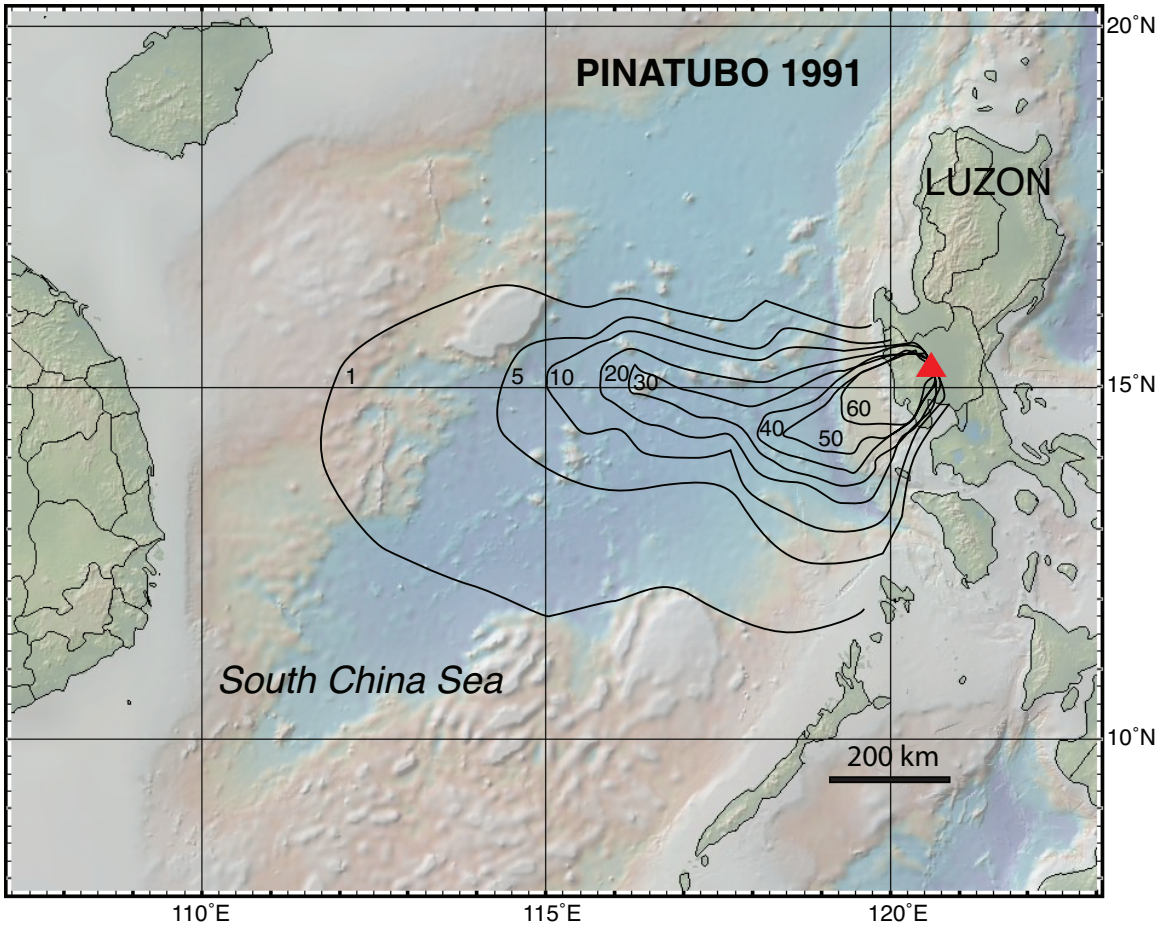

Figure 4b

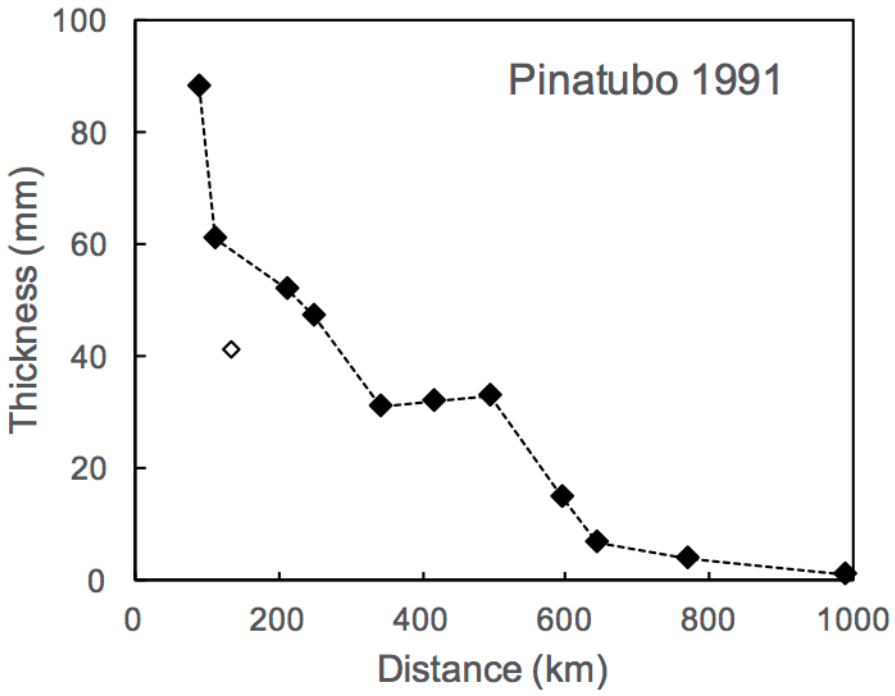
Pinatubo 1991
Thickness (mm)
Distance (km)
0
20
40
60
80
100
0
200
400
600
800
1000

Figure 5. June 1991 tephra deposit. (a) Plot showing movement of the ash cloud front (gray crosses) and airborne fine ash mass (black diamonds) as a function of time from the start of the eruption (which lasted for 9 hours). All measurements are from satellite data presented in Guo et al. (2004). (b) Deposit grain size distributions as a function of distance along deposit axis, show as sample mass <63µm (very fine ash), 32µm (nominal upper limit for satellite detection) and 2µm (respirable). Data from Wiesner et al. (2004).

Figure 5a

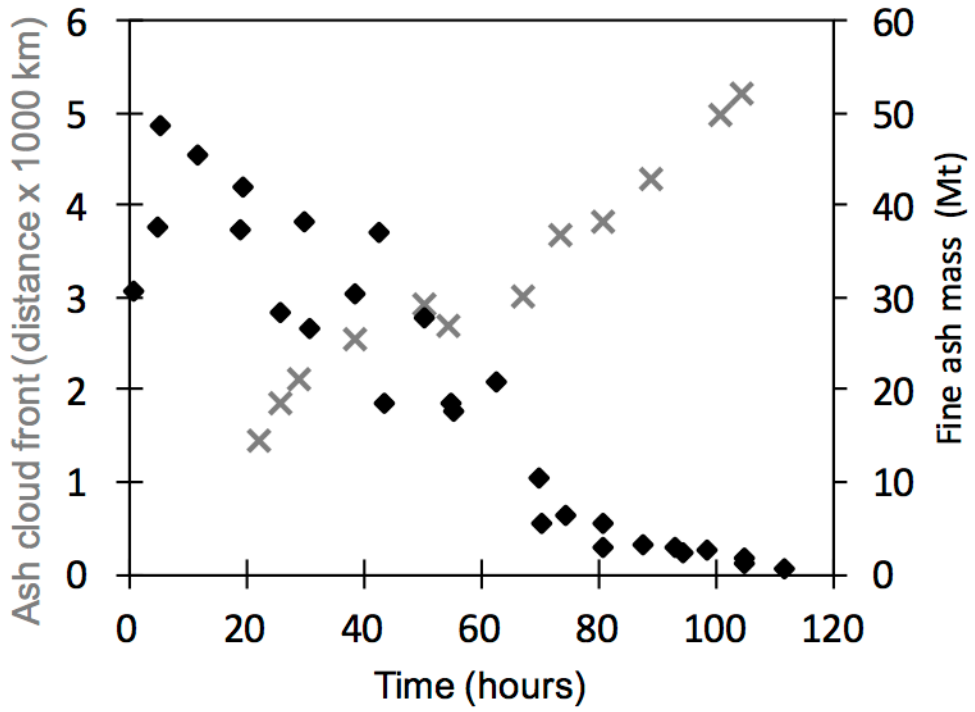

Figure 5b

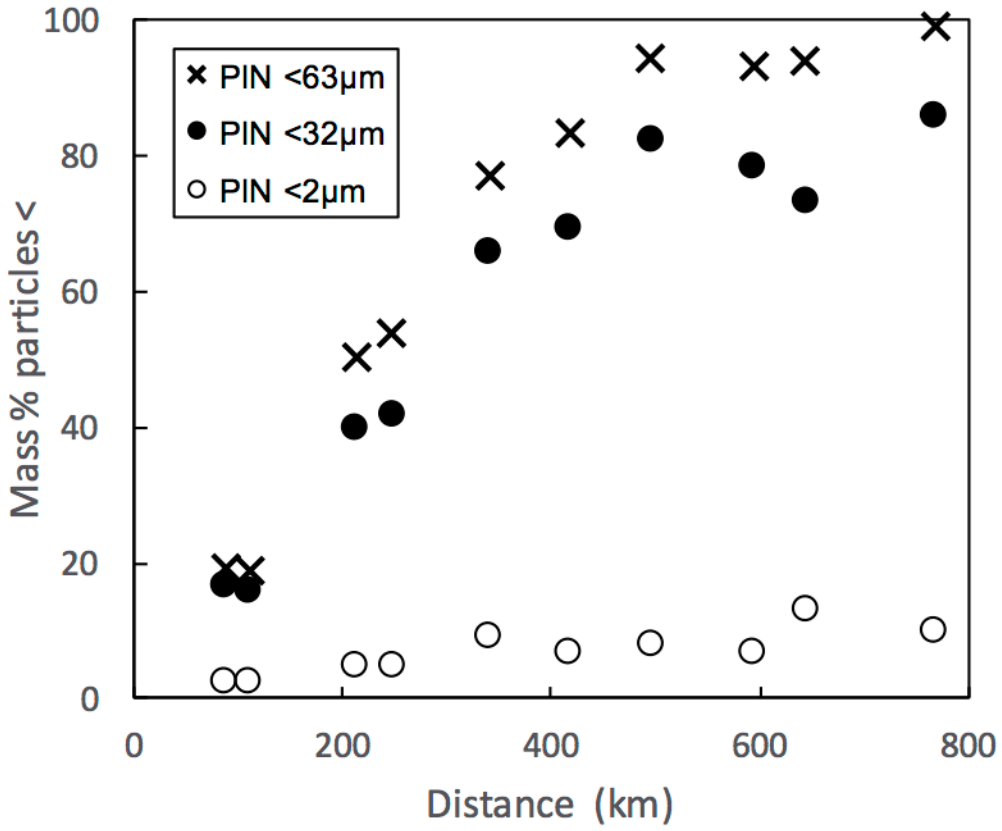
PIN <63µm
PIN <32µm
PIN <2µm
Mass % particles <
100
80
60
40
20
0
0
200
400
600
800
Distance (km)

Figure 6. Map showing ash cloud coverage and distal tephra locations for the 2010 eruptions of Eyjafjallajokull, Iceland. Sites are separated by maximum observed particle size (> 20µm or <20µm; most of the ≤20µm sites are data from PM10 monitors. Data from Gundmundsson et al. (2012), Stevenson et al. (2012), Swindles et al. (2013); background map made using GeoMapApp (www.geomapapp.org).

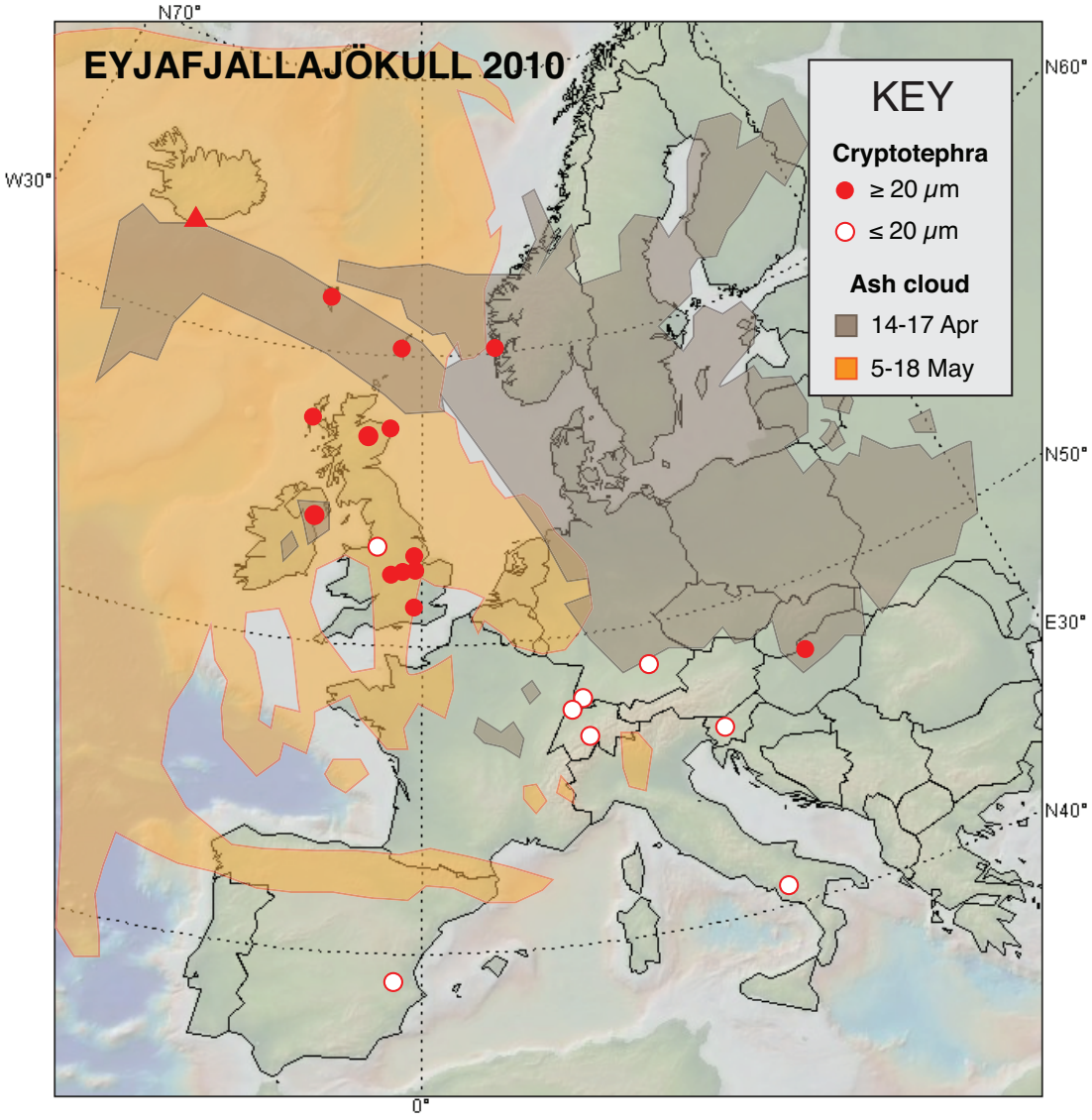

Figure 7. Tephra deposit produced by the 1875 eruption of Askja, Iceland. (a) Isochrones of first ash fall determined from eyewitness accounts (locations shown by blue circles); times are local time in Scandanavia, starting on 29 March. Reproduced from Mohn (1877). (b) Isopach map for the deposit reproduced from Carey et al. (2010; solid red lines) and modified using data collated here (purple dashed lines). Additional pseudo-thickness data provided as numbers (in µm) next to black dots (when average shard size is assumed to be 100µm) and gray dots (when average shard size is assumed to be 40µm). Arrow labeled KB points to Klockan Bog location referenced in text. All data sources and thickness calculations provided in Supplementary Material. Background map made using GeoMapApp (www.geomapapp.org).

Figure 7a

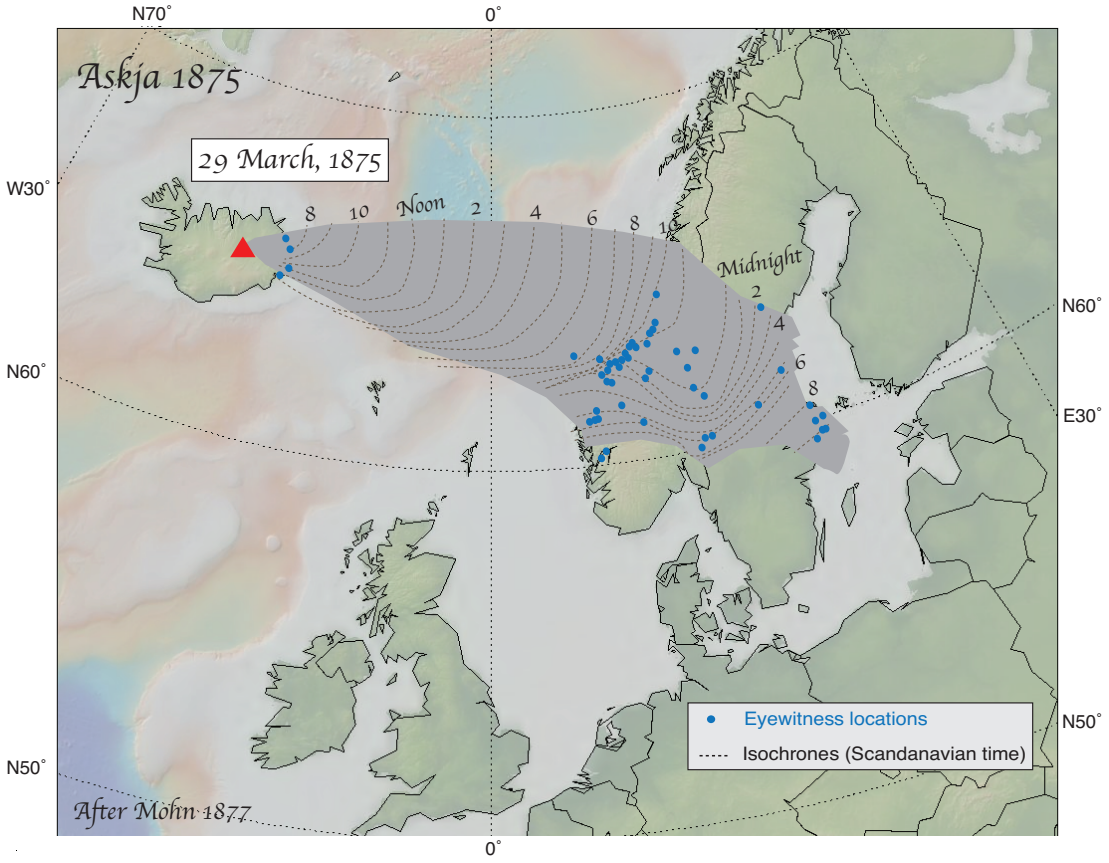

Figure 7b

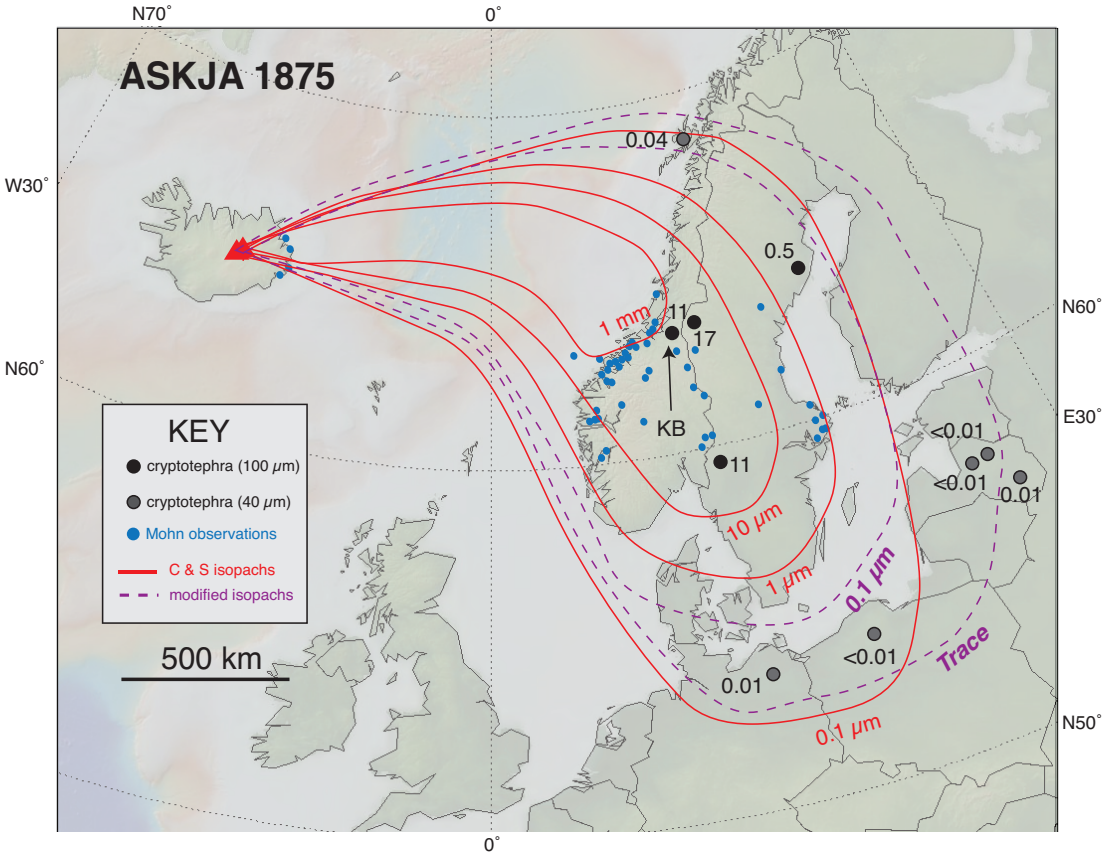
ASKJA 1875
N70˚
0˚
W30˚
N60˚
N60˚
E30˚
N50˚
0˚
0.04
0.5
1 mm
11
17
KB
11
10 µm
1 µm
0.1 µm
Trace
<0.01
<0.01
0.01
<0.01
0.01
0.1 µm
KEY
cryptotephra (100 µm)
cryptotephra (40 µm)
Mohn observations
C & S isopachs
modified isopachs
500 km

Figure 8. Tephra deposit produced by, and cryptotephra associated with, the White River Ash east (WRAe) eruption. (a) Map showing location of mapped deposit (in gray, from Lerbekmo, 2008) and cryptotephra locations (red circles, from Jensen et al., 2014). Nordan's Pond Bog is the only location with shard counts and particle size measurements (Pyne-O'Donnell et al., 2012). Background map made using GeoMapApp (www.geomapapp.org). (b) Thickness-distance measurements for WRAe (data from Lerbekmo, 2008; Pyne-O'Donnell et al., 2012) and 1875 Askja (data from Fig. 7b).

Figure 8a

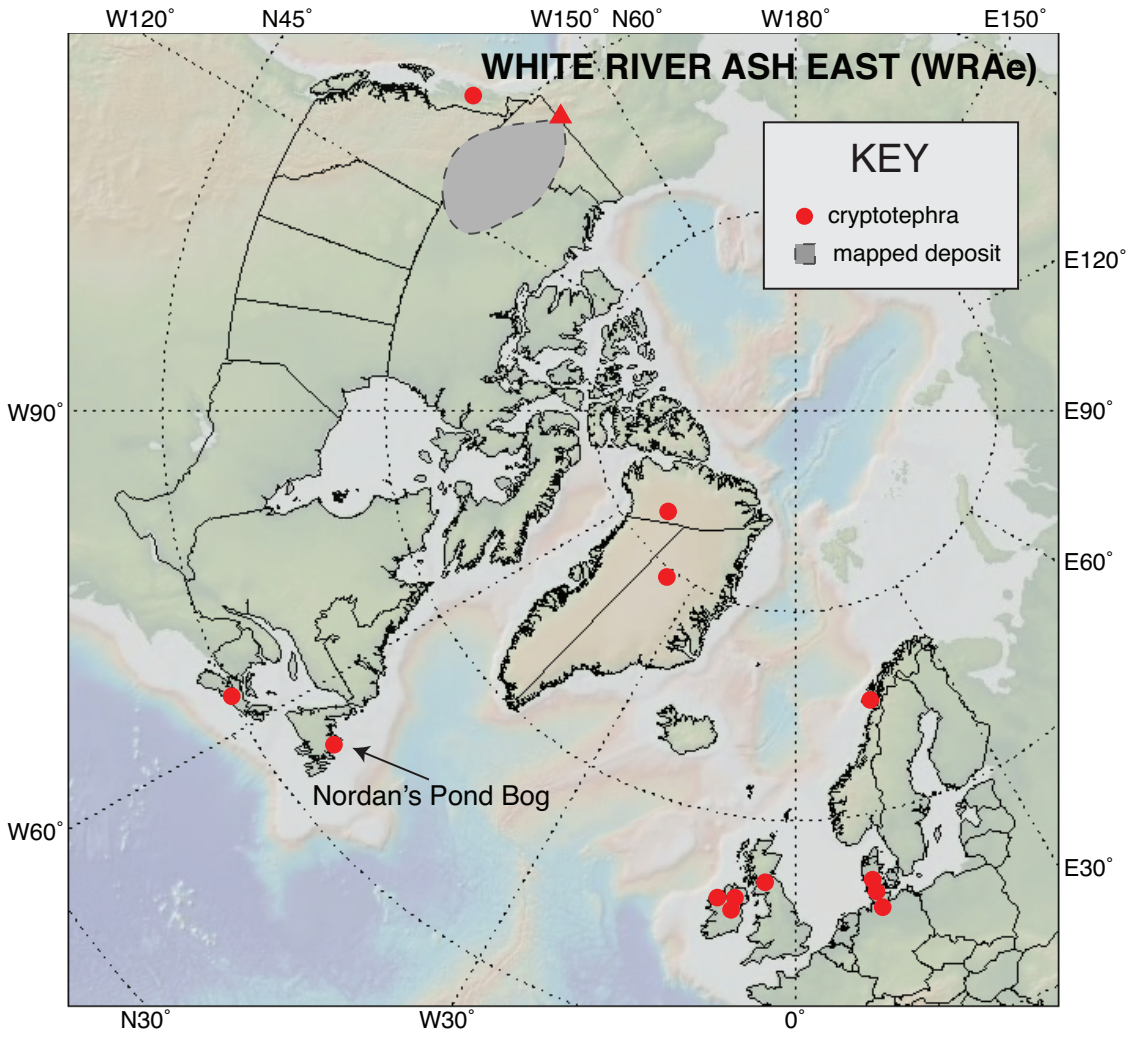

Figure 8b

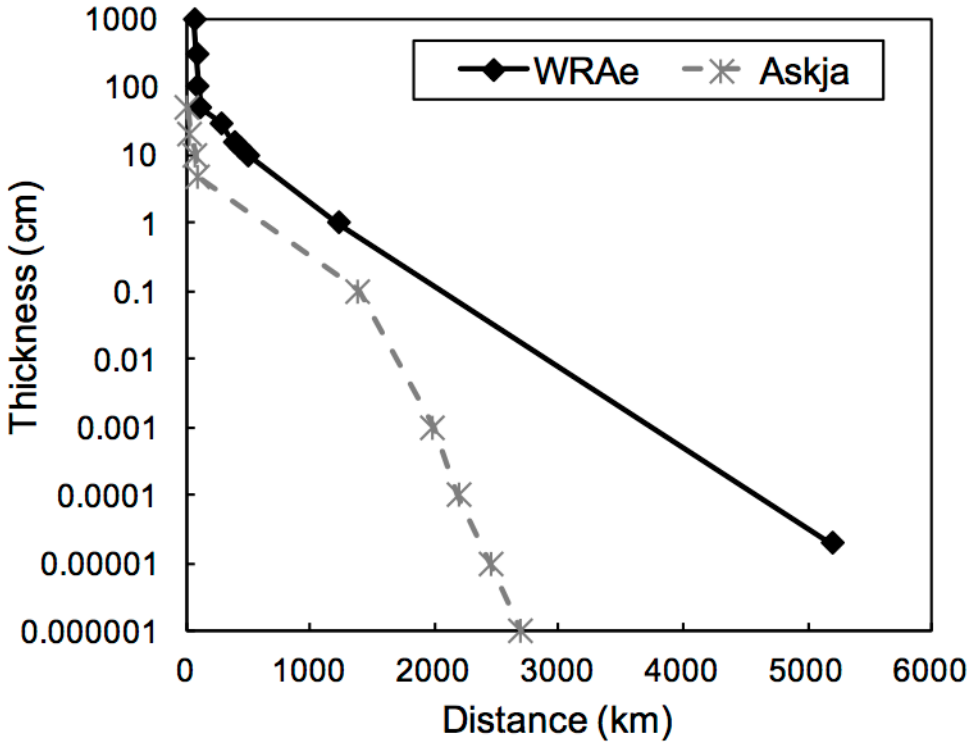
1000
100
10
1
0.1
0.01
0.001
0.0001
0.00001
0.000001
Thickness (cm)
WRAe
Askja
0
1000
2000
3000
4000
5000
6000
Distance (km)